

# A successful resimulation of the 7–8 January 2005 winter storm through initial potential vorticity modification in sensitive regions

By B. RØSTING<sup>1\*</sup> and J. E. KRISTJÁNSSON<sup>2</sup>, <sup>1</sup>The Norwegian Meteorological Institute, P.O. Box 43 Blindern, N-0313 Oslo, Norway; <sup>2</sup>Department of Geosciences, University of Oslo, Norway

(Manuscript received 13 September 2007; in final form 10 March 2008)

## ABSTRACT

In this study, we present an example of the benefit that can be achieved from carefully designed manual modification of a numerical weather prediction analysis. The case to be investigated is the severe winter storm of 7–8 January 2005, affecting the North Sea and southern Scandinavia. Modifications of potential vorticity (PV) fields according to features in water vapour (WV) images are combined with information from singular vectors (SV) in an attempt to improve the initial state over data sparse regions west of the British Isles. The apparent mismatch between features in the WV image and the upper level PV anomalies in the numerical analysis is corrected, mainly at levels indicated as sensitive by the fastest growing SVs, in order to maximize the impact on the simulation. Model reruns, based on the inverted corrected PV fields, were then performed. The manual correction of PV fields led to a substantial improvement of the simulations of the storm. The PV modifications were carried out by a digital analysis system, implemented at the Norwegian Meteorological Institute. This system allows the PV modifications to be done interactively within an operational time limit.

## 1. Introduction

The quality of the state of the art numerical weather prediction (NWP) models has improved substantially over the last decade. This is to a great extent due to improved physical parametrizations, higher horizontal and vertical resolution and improved methods for assimilation of satellite data, for example, 4D-Var. (Rabier et al., 2000; Bouttier and Kelly, 2001). Hence, severe storms over the Atlantic and Pacific oceans are now generally caught well by current NWP models. However, forecast failures still take place and when they occur they tend to involve cases of rapid cyclogenesis which may cause substantial damage and threaten human life. In such cases, though they may be scarce, there should be an option for the human forecaster to intervene manually by correcting errors in the numerical analysis followed by a rerun of a numerical model. A promising tool for manual interference is the correction of the potential vorticity (PV) field in the NWP analysis according to information inferred from water vapour (WV) images. After correction of PV in a numerical analysis a new analysis is obtained by inverting the corrected PV field (e.g. Demirtas and Thorpe, 1999; Browning et al., 2000; Røsting

et al., 2003; Hello and Arbogast, 2004; Røsting and Kristjánsson, 2006). This method yields a balanced analysis containing height and wind fields which are consistent in three dimensions.

Modified PV fields obtained manually may also be subjected to variational analysis as shown by Verkley et al. (2005). This is done by preparing a new cost function which contains a term analogous to the observation term, measuring the distance between the modified PV field and the original model PV. The error covariance matrix contains errors of the PV field retrieved from the original analysed NWP PV field. The background term in this new version of the cost function is identical to the ordinary cost function used in the assimilation. This method has yielded promising results in some case-studies.

Objective methods to improve the initial state of numerical simulations have been performed. These methods are:

- (i) The ensemble-transform Kalman-filter targeting guidance (ETKF) (e.g. Bishop et al., 2001; Majumdar et al., 2002).
- (ii) The singular vector (SV) technique (e.g. Buizza and Palmer, 1995).

The ETKF method is based on identifying regions where assimilation of new data (e.g. from dropwindsondes during flight campaigns), will reduce the analysis error covariance within the verification region. The technique adopts an ensemble of numerical forecasts from which the differences between the individual

---

\*Corresponding author.  
e-mail: bjorn.rosting@met.no  
DOI: 10.1111/j.1600-0870.2008.00329.x

forecasts and the average of the forecasts are determined. These differences determine the analysis error covariance matrix. Hence the error statistics is flow dependent.

The SV technique adopts adjoint methods and is in this study based on the total energy norm. The leading SVs indicate regions in the atmosphere that are sensitive to perturbations of the flow. Small errors in the NWP analysis or additional observations in such regions will strongly influence the NWP simulation. Hence, like the ETKF method, the SVs identify regions where new observations may be beneficial for the numerical simulation (Montani, 1998; Buizza and Montani, 1999; Montani et al., 1999; Jung et al., 2005).

In our investigations the numerical reruns based on the new analysis obtained by PV inversion are performed without invoking assimilation. The corrections of the NWP analysis fields are frequently large and may for that reason be rejected by the assimilation routines. The SV method determines the degree of sensitivity in regions subject to PV corrections. Combined use of WV images, PV and SV analysis in correcting numerical analyses has produced improved reruns of some severe storms, as demonstrated in Browning et al. (2000), Røsting et al. (2003) and Røsting and Kristjánsson (2006).

The main purpose of this paper is to describe a rerun of the 7–8 January 2005 storm by initial PV modification according to combined information derived from WV images and SVs. Though this storm was forecast rather well by the operational NWP models in the short range, there were forecast errors in track, propagation speed and deepening rate of the cyclone in some operational numerical simulations. Inspection of the WV image revealed a mismatch between the expected location of NWP PV anomalies retrieved from the Norwegian High Resolution Limited Area Model (HiRLAM) and features observed in the WV image.

In Section 2, some basic theoretical concepts and methodology are provided while a brief synoptic description of the 7–8 January storm is presented in Section 3. The operational HiRLAM simulation of the storm and some other simulations are described in Section 4. Section 5 describes SV analysis related to the cyclone development, while PV modifications and numerical reruns are presented in Sections 6 and 7. Discussion and conclusions are given in Sections 8 and 9, respectively.

## 2. Theory and methods

### 2.1. Potential vorticity

A key concept in our study is Ertel's potential vorticity which is given by

$$q = \frac{1}{\rho} \boldsymbol{\eta} \cdot \nabla \theta, \quad (1)$$

where  $\rho$  is air density,  $\boldsymbol{\eta}$  is the absolute vorticity vector and  $\nabla \theta$  is the three dimensional gradient of potential temperature. PV is expressed in PV-units, defined as  $1 \text{ PVU} = 10^{-6} \text{ m}^2 \text{ s}^{-1} \text{ K kg}^{-1}$ .

Changes of PV for an air parcel are due to diabatic effects and friction, and the budget of PV confined within a specific volume  $\tau$  is described by

$$\frac{D}{Dt} \left( \int \int \int_{\tau} q \rho d\tau \right) = \int \int_S (\dot{\theta} \boldsymbol{\eta} + \theta \mathbf{F}_r) \cdot \mathbf{n} dS \quad (2)$$

(Hoskins et al., 1985).

Here  $S$  is the bounding surface of the volume  $\tau$  and  $\mathbf{n}$  is the unit vector perpendicular to the surface,  $\mathbf{F}_r$  is the friction force,  $\theta$  is potential temperature and  $\dot{\theta}$  denotes diabatic heating.

This relation shows that the mass integrated PV contained within a volume changes due to diabatic effects and friction on the surface of the volume only. Diabatic effects and friction within the volume will merely redistribute PV contained within it, preserving the total mass integrated PV. When latent heat is released in a confined region, that is, associated with ascending motion within a developing cyclone, PV will be redistributed within the cyclonic vortex. The spatial orientation of such a diabatically modified PV structure assumes the shape of a PV dipole, with a positive (negative) PV anomaly below (above) the diabatic heating maximum (e.g. Shutts, 1990). The low level PV anomalies tend to be advected by the winds around the cyclone, contributing to the strong low level winds observed at the rear of intense extratropical cyclones.

In the manual corrections of the PV fields described later in this paper, PV modifications were not constrained according to relation (2). One may, however, guided by relation (2), try to make the PV corrections more consistent by e.g. letting reductions of upper level PV consistent with a cloud head observed in the WV satellite image be accompanied by enhanced low level PV close to the surface cyclone and associated front. This means that in the present study we adopt features from conceptual models of explosive cyclogenesis rather than stringent use of eq. (2).

### 2.2. Singular vectors

SVs are calculated by adjoint methods in order to highlight sensitive regions in the atmosphere (e.g. Buizza and Palmer, 1995; Kalnay, 2003).

SVs ( $\mathbf{v}_i$ ) are ranked according to their growth rate ( $\mathbf{v}_1, \mathbf{v}_2, \dots, \mathbf{v}_n$ ). The vectors  $\mathbf{v}_i$  form an orthonormal basis in phase space. Here  $\mathbf{v}_1$  represents the most unstable direction in phase space,  $\mathbf{v}_2$  the second most unstable direction and so on. If  $\mathbf{L}$  is the tangent linear operator, the SVs evolve according to  $\mathbf{L}\mathbf{v}_i = \sigma_i \mathbf{u}_i$ , where  $\mathbf{v}_i$  and  $\mathbf{u}_i$  are the initial and evolved SVs, respectively. The singular values are denoted by  $\sigma_i$ . The initial SVs ( $\mathbf{v}_i$ ) are stretched (contracted if  $\sigma_i < 1$ ) by an amount equal to  $\sigma_i$  and rotated to become parallel with the evolved SVs ( $\mathbf{u}_i$ ) over a specific time interval ( $t_0, t_1$ ), referred to as the optimization time interval, see for example, Kalnay (2003) for details. Any perturbation of the flow at initial time,  $\delta \mathbf{x}(t_0)$ , can be expressed as  $\delta \mathbf{x}(t_0) = \sum_{i=1}^n \langle \delta \mathbf{x}_0, \mathbf{v}_i \rangle \mathbf{v}_i$ . Here we used the inner product which for any vectors  $\mathbf{a}$  and  $\mathbf{b}$  is written as  $\langle \mathbf{a}, \mathbf{b} \rangle$ . A similar relation

can be written for the perturbation  $\delta \mathbf{x}(t_1)$  at optimization time, using the evolved SVs ( $\mathbf{u}_i$ ).

For targeted SVs the optimization time interval is the time needed for the fastest growing SV to reach maximum amplitude, given by their singular values, within a predefined verification region. For instance in the present investigation we are seeking the region which contains the SVs (target area) that will reach peak amplitude over the North Sea and southern Scandinavia (verification region) in 18 h. The verification region contains the cyclone at maximum intensity 18 h ahead.

The calculation of SVs is based on linear dynamics (the tangent linear propagator and its adjoint) and simplified physics, hence they may fail to describe properly the sensitive regions where highly non-linear processes involving release of latent heat occur (Montani et al., 1999). SVs are, however, designed to represent strong energy growth. SVs may be presented graphically by fields of streamfunction, geopotential heights, temperature or in terms of PV.

The three dimensional structure of the SVs indirectly offers information on the sensitivity of the flow to new observations. Hence corrections (e.g. modification of PV) in such sensitive areas are likely to have a large impact on the simulation.

A SV is assumed to change according to

$$\frac{Dq'}{Dt} \equiv (\partial/\partial t + \bar{\mathbf{u}} \cdot \nabla)q' = -\mathbf{u}' \cdot \nabla \bar{q} \quad (3)$$

(Montani, 1998). In this equation  $\bar{q}$  and  $\bar{\mathbf{u}}$  represent the basic state PV and three dimensional velocity vector, respectively, changing slowly with time, while  $q'$  and  $\mathbf{u}'$  denote perturbations of the flow, that is, perturbation PV and three dimensional perturbation velocity vector, respectively.

Hence the SV (represented by the PV perturbation  $q'$ ) is modified by exchanging potential vorticity with the basic state flow. The basic state flow has strong PV gradients at the sloping tropopause near the jet streams and at strong low level fronts. In such regions of strong basic state PV gradients SVs tend to grow or decay depending on the PV structure of the basic state flow and of the asymmetry of the perturbation itself (e.g. Røsting and Kristjánsson, 2006).

A further justification for describing SV dynamics by relation (3) is provided in Section 8 below.

### 2.3. Data and forecasting tools

The boundary fields for our experimental runs are retrieved from the European Center for Medium range Weather Forecasts (ECMWF) and PV is calculated on pressure surfaces from these fields. The calculation is carried out at the WMO mandatory levels<sup>1</sup> by HiRLAM with 50 km grid spacing and 31 model levels, for region 1 in Fig. 1. Modifications of PV and PV inversion

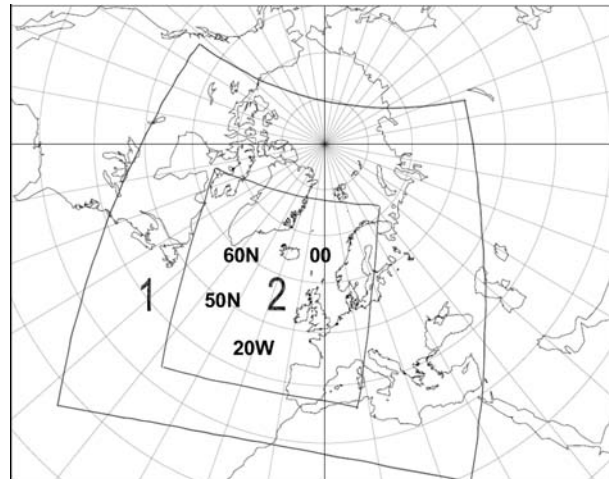


Fig. 1. Model area for the experimental simulations by HiRLAM with 20 km horizontal grid spacing and 40 model levels, indicated by region 2. The HiRLAM boundary fields are provided for the area 1 with the coarser resolution (50 km, 31 model levels). PV inversion is carried out in a region somewhat smaller than the large area 1.

are performed for a somewhat smaller area.<sup>2</sup> The new simulations of the storm are carried out by a version of HiRLAM with 20 km grid spacing and 40 model levels in region 2 shown in Fig. 1. SVs, based on the energy norm, are calculated by the ECMWF PrepIfs System ECMWF, Newsletter (1999), using a spectral model T42L31.

The modification of PV is performed interactively by using the Digital ANALYSIS (DIANA) system which is used operationally at the Norwegian Meteorological Institute (MI). Various numerical fields from a variety of NWP models from several meteorological centres, together with observations including satellite and radar images are retrieved in DIANA. This system comprises an efficient forecasting tool including production of synoptic surface analyses. DIANA has been modified to allow modification (subjective analysis) of PV and relative humidity (RH) fields on pressure surfaces to be done interactively.

### 2.4. PV modifications and inverted fields

In this study, we describe two key points on which manual modification of PV in a NWP analysis are based:

(1) Air with stratospheric origin is very dry, while tropospheric air is frequently moist. Due to the strong absorption and emittance of radiation by water vapour in the wave range 6.2–6.7  $\mu\text{m}$ , dry regions in the atmosphere, allowing radiation from low and generally comparatively warmer levels to reach the satellite, appear dark, while moist regions and clouds, allowing radiation only from higher and colder levels to be recorded, are

<sup>1</sup> 1000, 900, 800, 700, 600, 400, 300, 250, 200, 150, 100 hPa.

<sup>2</sup> The smaller area was originally chosen for economical reasons, requiring a more limited integration region.

bright in the WV image. The highest sensitivity of these WV channels is normally located at 400 hPa. At this level humidity gradients are most clearly seen as different grey shades in the WV image (e.g. Weldon and Holmes, 1991; Santurette and Georgiev, 2005).

In dynamically active zones associated with the baroclinic areas, dark regions in the WV image correspond to dry stratospheric air with large PV values, and the darkest features are often associated with cyclonically curved PV contours. Such features are frequently identified as dry intrusions associated with rapid cyclogenesis (e.g. Weldon and Holmes, 1991; Browning, 1997). The bright regions are connected with moist tropospheric air with low upper level PV values. In case of cloud heads PV contours at the tropopause and lower stratosphere tend to be anticyclonically curved across the bright area. However, the degree of such anticyclonic curvature depends on the stage of cloud head development. In the mature stage of cyclogenesis the strongest PV gradients are aligned along the edge of the cloud heads.

Hence, in the baroclinic zones there is a strong relation between dark and bright regions in the WV images and the upper level PV field. This relationship is well documented (e.g. Appenzeller and Davies, 1992; Mansfield, 1996; Santurette and Georgiev, 2005).

Low level positive PV anomalies are frequently associated with bright regions, but the locations of such anomalies are difficult to infer from the satellite imagery alone, suggesting the use of knowledge derived from conceptual models and singular vectors.

(2) The sensitivity of the flow to error growth and hence to additional observations can be assessed by adopting, for example, the SV or ETKF techniques. By comparing these two techniques Majumdar et al. (2002) have demonstrated that the two methods to some extent highlight the same regions as sensitive to new targeted observations, that is, dropwindsondes, given the same verification area. The similarity of the methods is mainly observed on large scales. However, due to the differences of the techniques on which these methods are based the ETKF signal does not exhibit a vertical tilt sloping upstream as for initial SVs (Petersen et al., 2007). The ETKF signal usually covers a much larger geographical region than the SV signal. This is ascribed to:

(i) Error covariance length scales can be large in baroclinic zones.

(ii) The number of elements in the Kalman filtering error covariance matrix is based on the number of ensemble members of the NWP forecast, and this number is lower than the number of the rank of freedom of the NWP model (e.g. Kalnay, 2003). Hence the error covariance matrix is rank deficient and spurious errors in the ETKF signal may occur.

On the other hand, as mentioned in Section 2.2, SVs are based on linear dynamics and simplified physics, this may be a limitation to the use of targeted SVs as a tool in identifying the

true sensitive region. Also, the rather crude horizontal resolution (for economical reasons) of the SVs calculated in this study may cause inaccurate targeting (Montani et al., 1999).

Hence there are no indications that one of the methods is more useful than the other in identifying regions that are sensitive to targeted observations.

SVs are used in our research in identifying sensitive regions for the following reasons:

(i) We are modifying numerical PV-fields in sensitive regions, rather than adopting additional observations.

(ii) We do not include assimilation routines in our numerical reruns.

(iii) The SV method is readily available by the PrepIfs System referred to in Section 2.3.

The leading SVs (i.e. usually SVs 1–5) indicate regions in the atmosphere that are sensitive to perturbations of the flow (cf. Section 2.2). Such perturbations, representing analysis errors or corrections due to additional observations, tend to grow rapidly and will consequently have a strong impact on the NWP simulation. The vertical structure of PV modifications, that is, the levels where PV modification is performed, may be guided by the SV signal provided that such a signal exists in the region of interest. SV signals may be particularly useful in deciding on the PV modifications in the lower troposphere.

If SVs fail to show any signal in the region indicated as sensitive by the satellite image (i.e. the tell tale features of cloud head and dry intrusion), PV is modified according to the typical PV structure observed in many observational studies and successful NWP simulations of cyclogenesis, that is, adopting knowledge from conceptual models (e.g. Shapiro et al., 1999).

After completing the PV modification according to information retrieved from the actual WV image and members among the leading SVs, the PV fields are inverted using the inversion method developed by Davis and Emanuel (1991) and Davis (1992). The inversion technique is based on eq. (1) and Charney's balance condition (Charney, 1955) in spherical coordinates, horizontal boundary conditions are given by the hydrostatic relation, while vertical boundary conditions are supplied by the geopotential and the streamfunction. This PV inversion system handles flow with strong curvature and hence large Rossby number ( $\sim 1$ ). The Ertel PV is non-linear and for that reason PV anomalies cannot be inverted to yield unambiguously the total flow by summing up the height fields from all PV anomalies. However, a mathematical method developed by Davis (1992) allows the piecewise PV inversion to yield the total field, more accurately than inversion of quasi-geostrophic PV. This system of equations is not balanced for negative PV. In such conditions the method fails in describing the fields properly. A procedure to deal with this problem technically is described below.

The new analysis obtained by PV inversion contains balanced fields and, as mentioned above in the introduction, is adopted directly in the numerical rerun without invoking data assimilation.

Thus the method has an advantage of being capable of dealing with large analysis errors. Assimilation routines (3-4D-Var) may reject the corrected fields obtained by PV inversion if they deviate too much from the error statistics contained in the error covariance matrix used in the cost function.

Though the PV inversion method used here is based on the Ertel PV, representing the flow much better than quasi-geostrophic PV, there are limitations of the method which must be kept in mind:

(i) As mentioned above, PV inversion requires positive or zero PV everywhere. In case of regions containing (slightly) negative PV as retrieved from the HiRLAM simulations, a numerical technique which allows the iteration to converge is adopted (Kristjánsson et al., 1999). In such regions, however, the height fields obtained by PV inversion tend to deviate much from the observed height fields (as much as 80–120 m in some cases).

(ii) The PV inversion method used in this investigation yields geopotential heights and winds, but only non-divergent winds. This may be a source of errors in the resimulations. In several previous experiments with different cases, the neglect of the divergent winds in the analysis may have been reflected by a lack of deepening or even filling of the developing baroclinic wave in the first 3 h of the simulation. This is probably due to the fundamental importance of the divergence to change vorticity. After  $\sim 3$  h of simulation time, however, deepening starts and divergence is restored in all cases (Røsting and Kristjánsson, 2006). By enhancing low level PV anomalies, the tendency of filling appears to become reduced or even disappear. This positive effect is most likely due to the divergent winds associated with advection of the modified low level PV anomalies introduced in the analysis.

The fields obtained by PV inversion are checked against the observations. Since PV inversion yields geopotential heights of pressure surfaces and winds on pressure levels, interpolation to surface pressure is done. If necessary the procedure is repeated by further adjustment of the modified PV anomalies until the modified fields are as close to the observed as desired. By interactive methods, for example, performing the PV modifications on the DIANA system, such a manual ‘iteration’ of the PV field can be carried out within a reasonably short time, that is, an operational time limit. Most of the time needed to obtain a new numerical analysis depends on the time needed for performing the PV modification, that is, subjective analysis of the PV field at selected pressure levels, while running the PV inversion routine for the analysis time takes only 1–2 min. Finally, rerunning the model on the supercomputer, retrieval and post-processing of data require about 15 min.

### 3. Synoptic description of the January 2005 storm

An early stage of the storm development is identified as a developing wave at the southwest tip of Ireland shown in

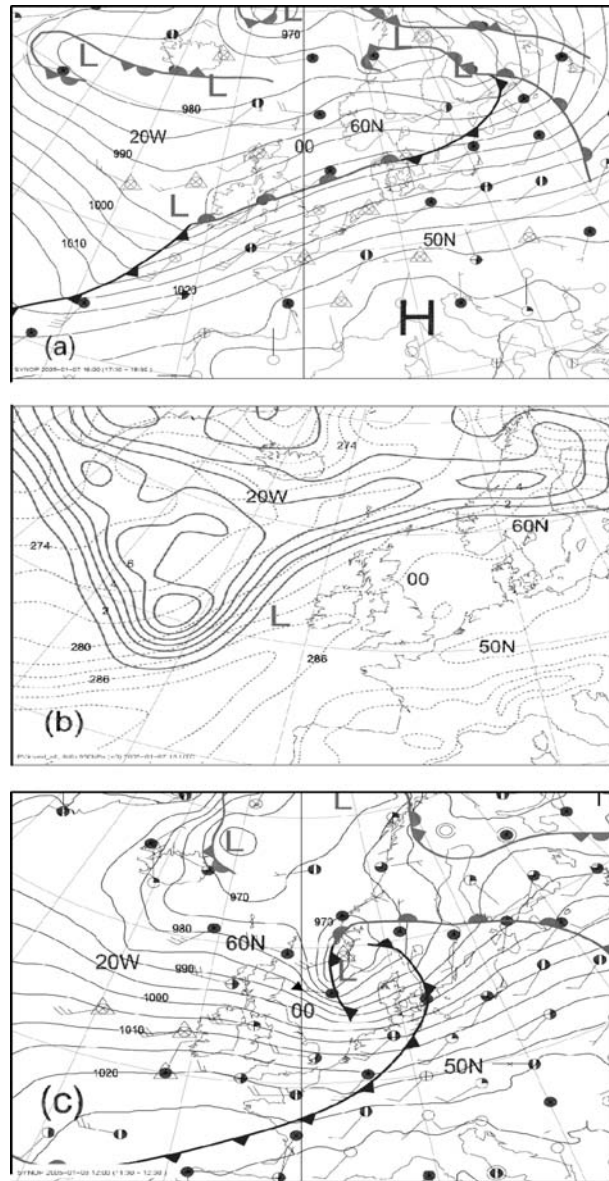


Fig. 2. (a) Synoptic analysis and observed 10 m winds at 18 UTC on 7 January 2005. (b) PV (bold contours) given in PVU on the 300 hPa surface and potential temperature on the 950 hPa surface (dashed contours), derived from the REHIR run. L denotes the location of the incipient low. (c) Synoptic analysis and observed 10 m winds at 12 UTC on 8 January 2005.

Fig. 2a. The figure presents the subjective analysis at 18 UTC on 7 January 2005. The winter storm, referred to as the Gudrun storm, developed rapidly between 18 UTC on 07 January and 00 UTC 08 January, as the incipient wave came under the influence of an upper level positive PV anomaly, Fig. 2b.

This development can readily be described as a (‘classical’) type B development, involving an upper level forcing, that is, upper level positive PV anomaly (at 300 hPa in Fig. 2b),

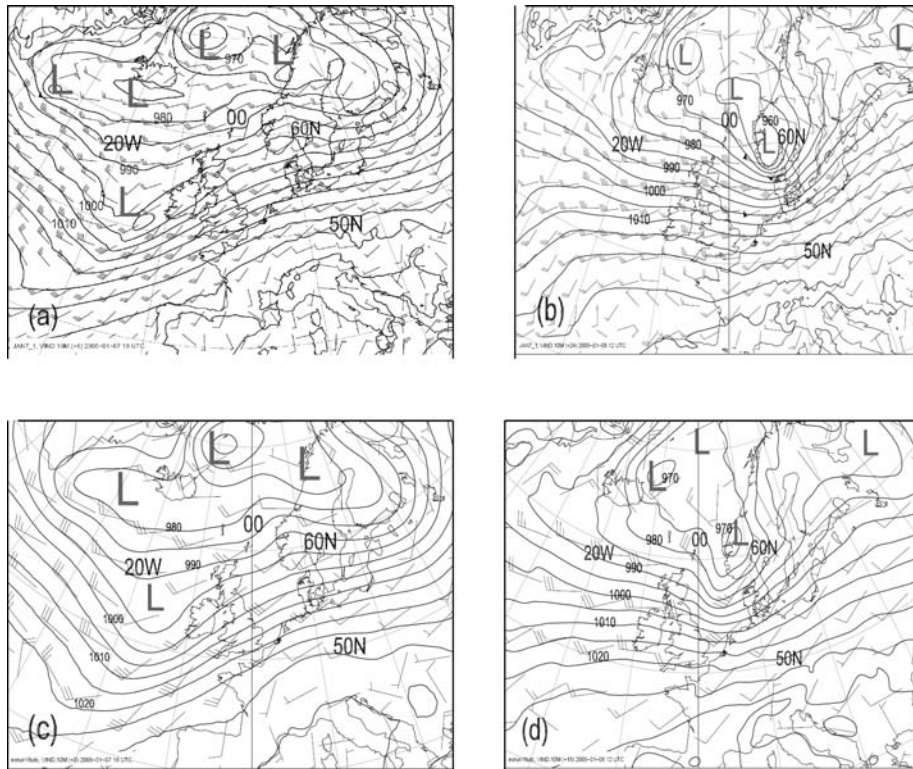


Fig. 3. (a) The 6 h HiRLAM forecast of surface pressure and 10m winds from the operational numerical analysis at 18 UTC on 7 January 2005. (b) The 24 h operational HiRLAM forecast of surface pressure and 10 m winds at 12 UTC 8 January 2005. (c) The REHIR analysis of surface pressure and 10m winds at 18 UTC on 7 January. (d) The REHIR 18 h simulation of surface pressure and 10 m winds valid at 12 UTC 8 January 2005, based on ECMWF analysis fields at 18 UTC 7 January 2005.

overrunning a low level frontal zone, identified by the 950 hPa potential temperature field in Fig. 2b, hence causing the frontal wave to grow. The storm reached peak intensity at 12 UTC on 8 January just off the western coast of Norway, with central surface pressure reaching  $\sim 960$  hPa, as seen in Fig. 2c. The strongest winds, exceeding  $25 \text{ m s}^{-1}$ , appeared over the North Sea (Fig. 2c). After making landfall there was no further deepening of the cyclone, but its central pressure remained nearly unchanged and strong winds exceeding  $25\text{--}30 \text{ m s}^{-1}$  affected large areas of southern Sweden and the Baltic States on 8–9 January.

#### 4. Some simulations of the storm

In this section, we study the results from the following simulations of the Gudrun storm:

(1) The operational Norwegian HiRLAM run (OPHIR) starting at 12 UTC on 7 January 2005. This simulation is performed for region 1 shown in Fig. 1.

(2) A HiRLAM rerun (REHIR) starting at 18 UTC on 7 January. This simulation is based on ECMWF boundary fields and is performed for the fine mesh region 2 shown in Fig. 1.

We have chosen to start REHIR and the experimental reruns in this investigation at 18 UTC on 7 January, because 6 h earlier, at 12 UTC available satellite images only partly cover the area of the upper level positive PV anomaly associated with the incipient cyclone.

Figure 3a shows the 6 h forecast surface pressure and 10 m winds by the OPHIR run valid at 18 UTC on 7 January. Compared to the synoptic analysis in Fig. 2a, there is a high degree of consistency with the observed surface field, except for slightly higher simulated pressure west of Ireland. Though this operational run predicted the track of the cyclone fairly well, comparison with the synoptic analysis at +24 h, valid at 12 UTC on 8 January, Fig. 2c, shows that the simulated storm, Fig. 3b, is too deep by  $\sim 5$  hPa and the forecast position is too far east, by about 250 km.

Figure 3c shows the NWP analysis of the REHIR run. The surface pressure west of Ireland, at the cyclone centre, is slightly too high, compared to the synoptic analysis shown in Fig. 2a. Figure 3d shows results from the REHIR simulation at +18 h, valid at 12 UTC on 8 January.

The forecast position was still too far east, by about 100 km, and the central pressure was too high by  $\sim 10$  hPa. Most notably, the simulated 10m winds at the rear of the cyclone

were strongly underestimated. The HiRLAM resimulation with ECMWF boundary fields and for the fine mesh region shown in Fig. 1, starting at 12 UTC was almost identical to REHIR (not shown).

The exaggerated deepening rate and too rapid propagation speed of the cyclone, as observed in the operational HiRLAM simulation starting at 12 UTC on 7 January (Fig. 3b) motivates an inspection of the three dimensional structure of the cyclone at 18 UTC. Though there was only a slight disagreement between the analysed surface pressure and observations at this time, there were indications of analysis errors at upper levels west of Ireland. The emergence of the cloud head and dry intrusion as observed in the WV image, indicated a mismatch with the NWP upper level PV fields, calling for an investigation of the sensitivity of the flow to perturbations and hence to PV modification in the area. This will be elaborated on in Section 6 below.

## 5. The sensitive areas

In order to assess objectively the degree of sensitivity of the flow across the North Atlantic to perturbations, and hence the degree of susceptibility of the flow to new observations, we now study the leading initial SVs valid at 18 UTC on 7 January. The targeted SVs are calculated with an optimization time of 18 h and with a verification region between 05°W and 10°E, 52–64°N. This means that the SVs are designed to reach peak amplitude 18 h ahead within the verification area. At +18 h the verification area contains the cyclone at its most intense stage of development.

Figure 4 shows the PV structure of SV 1 and SV 2 at levels 13 (~300 hPa), 16 (~400 hPa) and 24 (~850 hPa). The SVs show a widespread signal at upper levels (e.g. 13 and 16). By shrinking the verification area the initial SVs frequently become confined to smaller areas, though this did not occur at upper levels in this

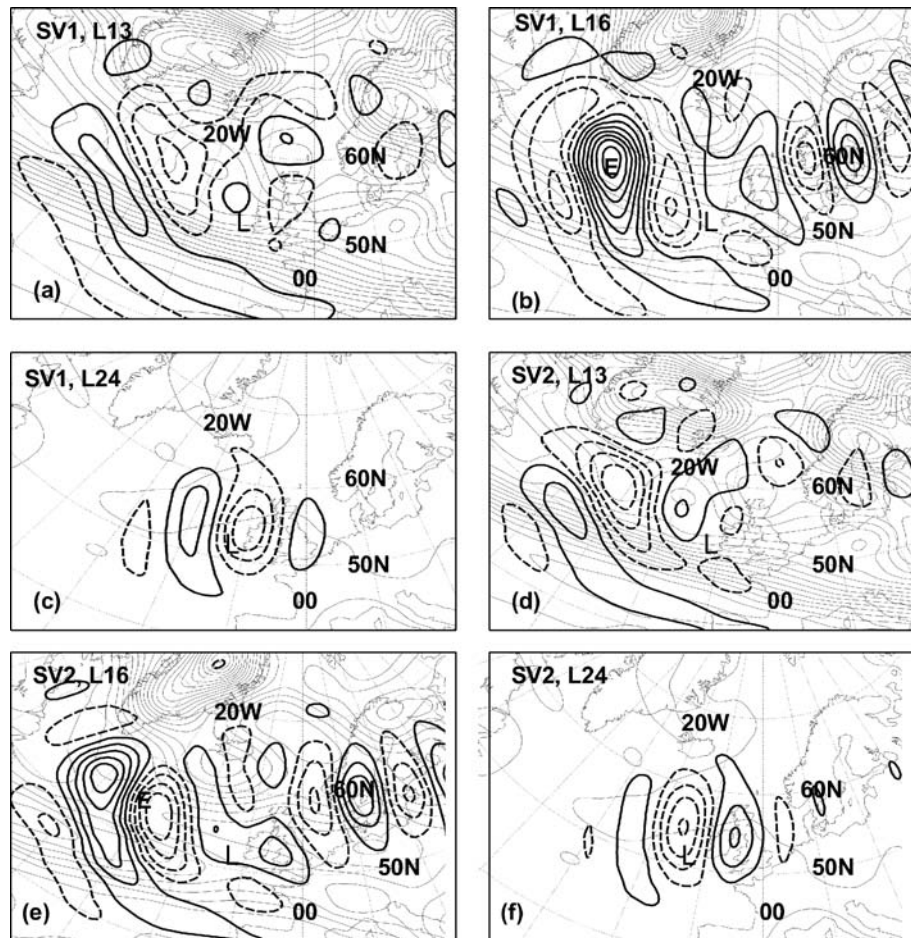


Fig. 4. Potential vorticity structure of singular vectors (SVs) 1 and 2 at 18 UTC on 7 January 2005, with optimization time of 18 h. Verification region between 05°W and 10°E, 52–64°N. (a) SV1 at level 13 (~300 hPa), (b) SV1 at level 16 (~400 hPa), (c) SV1 at level 24 (~850 hPa) (d) SV2 at level 13 (~300 hPa), (e) SV2 at level 16 (~400 hPa) and (f) SV2 at level 24 (~850 hPa) Bold solid (dashed) contours show the positive (negative) values of the SVs, contour interval 0.004 PVU. Thin contours depict basic state PV with contour interval 0.5 PVU. The position of the incipient cyclone is indicated by the letter 'L'. The letter 'E' indicates the region of PV modification in experiment 3.

case. However, due to the strong upper level winds associated with severe winter storms, effects arising from perturbations of the flow far upstream of the cyclone may reach the site of the cyclone in 24 h or less. This effect is reflected by the rather large-scale of the upper level SV signal seen in Fig. 4 and is expanded on in Section 8. The strongest signal is located over the mid-North Atlantic, at 20–40°W, 50–57°N, the region of maximum intensity denoted by the letter 'E' in Fig. 4b. It will be demonstrated below in Section 7 that perturbation of upper level PV in this region has a notable effect on the simulated development of the Gudrun storm. The SVs are strongly localized at lower levels, close to the incipient cyclone, as seen in Figs. 4c and f, indicating the importance of low level PV anomalies, associated with diabatic effects and friction, in deepening the cyclone.

The SVs 3–5 also point to the areas close to and upstream of the cyclone as sensitive (not shown), but less so than the first two SVs. We also note that the SVs are located in regions with strong gradients of basic state PV, particularly at upper levels, indicating that the conditions for growth of perturbations are favourable, according to the discussion related to relation (3).

In the case of the Gudrun storm the choice of verification area appeared to be important for the structure and location of the SVs. By extending the western boundary of the verification area to 15°W, leaving the remaining boundaries unchanged, the fastest growing targeted SVs showed very weak signals in the region near the cyclone (not shown). The reason for this is probably the presence of a second cyclone which developed rapidly into another severe winter storm, located just west of the British Isles on 8 January. Hence two strong cyclones were located within the verification region. The targeted SVs highlighted the second winter storm, which was stronger and of larger scale than the Gudrun storm.

## 6. PV modifications and reruns

### 6.1. The control PV run

Figure 5a shows the WV image (METEOSAT7) at 18 UTC on 7 January with the analysed (unmodified) PV contours at 400 hPa (bold contours) and 800 hPa (dashed contours) levels superimposed. The cloud head, with location indicated by B in Fig. 5a, has at this time acquired the classical feature of an incipient severe storm (e.g. Young et al., 1987). Though the PV contours at 400 hPa run partly anticyclonically across the cloud head B, they fail to match properly with the cloud head feature. Dry stratospheric air is seen at A in the image, Fig. 5a, suggesting a dry high-PV intrusion with stronger cyclonic curvature of upper level PV contours than seen in the PV field in this control analysis. The region of maximum PV is expected to be located closer to the dark region. At C low level PV is present in the same area as the strong localized SV signal (Figs. 4c and f).

We now perform a PV inversion of the unmodified PV field. The geopotential heights and winds obtained from the PV in-

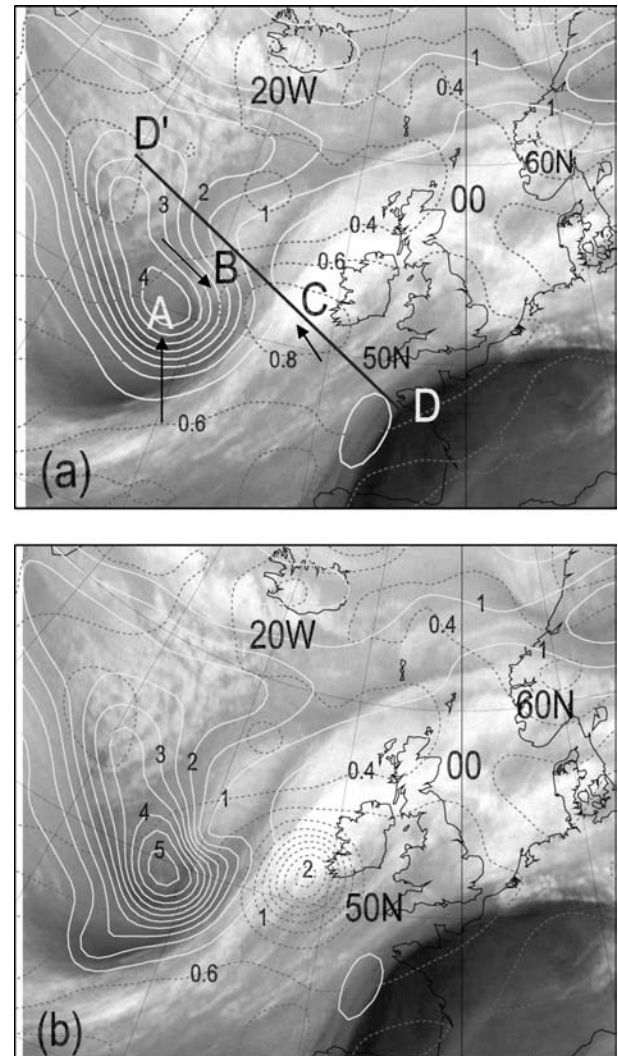


Fig. 5. (a) Control analysis of PV on the 300 hPa (solid contours) and 800 hPa (dashed contours) surfaces at 18 UTC 7 January 2005 superimposed on METEOSAT7 WV image for the same time. Arrows denote the modification regions. The bar DD' denotes the location of the cross-section discussed in the text. (b) Modified analysis of PV on the 300 and 800 hPa surfaces at 18 UTC 7 January 2005 superimposed on a METEOSAT7 WV image. Contour interval 0.5 PVU for upper level PV, 0.2 PVU for low level PV.

version yield, together with relative humidity fields, our control analysis. The moisture fields are retrieved from the ECMWF boundary fields at 18 UTC.

The numerical rerun based on this analysis is referred to as CONTROL. Fig. 6a shows the 18 h CONTROL simulation of the storm, valid at 12 UTC 8 January.

With regard to the cyclone centre CONTROL shows an improvement of location over OPHIR (the operational HiRLAM simulation at +24 h, Fig. 3b) and REHIR (the HiRLAM simulation with ECMWF boundary fields, Fig. 3d) at +18 h. The

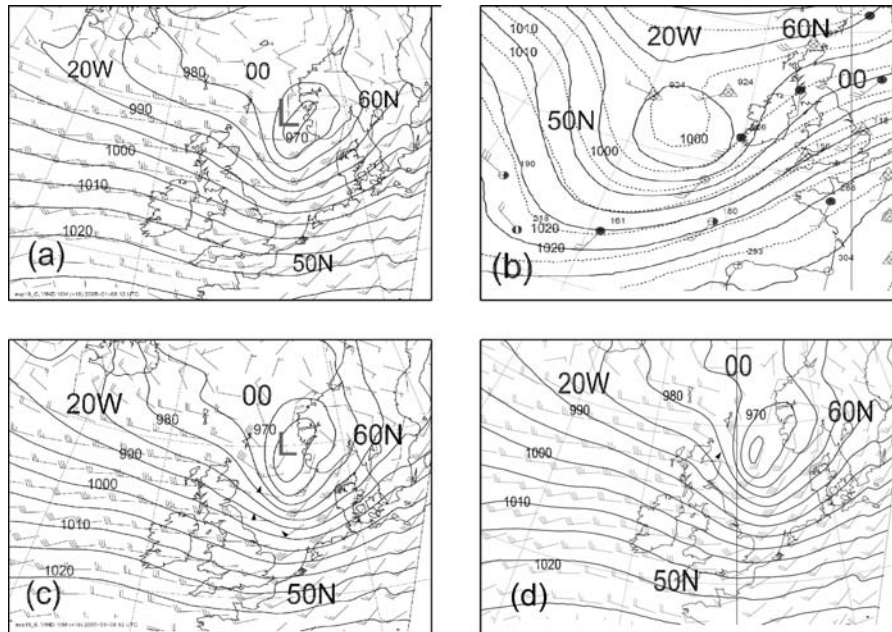


Fig. 6. (a) 18 h CONTROL forecast of surface pressure and 10 m winds at 12 UTC 8 January 2005, based on analysis from inverted original PV fields. (b) NWP CONTROL (dashed contours) and EXP1 (solid) analyses of surface pressure at 18 UTC on 7 January. (c) As in (a), but for the EXP1 run. d) As in (a), but for the EXP2 run.

cyclone centre is closer to the observed position, but the central pressure is higher than observed by about 10 hPa at +18 h. The winds are weaker than observed, as seen by comparison with Fig. 2c.

### 6.2. The modified PV run

We now modify the PV field according to information derived from the WV image and the SV analysis. The modification is performed at pressure levels indicated as sensitive by SV1 and SV2 (Fig. 4).

The arrows in Fig. 5a indicate the regions where PV is changed.

(i) PV is reduced in the cloud head at B at tropopause level,  $\sim 300$  hPa, and down to 500 hPa. As mentioned above, in Section 2.4, the WV signal in the  $6.2\text{--}6.7\ \mu\text{m}$  range is normally most sensitive to moisture gradients at 400 hPa. In order to explain the pronounced light grey shade of the cloud head, a relative humidity (RH) of  $\sim 70\%$  is likely to be present at the 400 hPa level (Santurette and Georgiev, 2005).

The cross-section DD' in Fig. 7a shows the Control analysis of RH at 18 UTC on 07 January across the polar front cloud band ( $08^\circ\text{W}$  to  $17^\circ\text{W}$ ) and the cloud head ( $18^\circ\text{W}$  to  $21^\circ\text{W}$ ), location shown in Fig. 5a. At the location of the cloud head RH reaches values in the range of only 30–40% at 400 hPa, while regions with 70–80% are located at and below 700 hPa underneath the cloud head. The WV channels  $6.2$  to  $6.7\ \mu\text{m}$  have weak sensitivity to moisture gradients at these low altitudes (Weldon and Holmes,

1991; Santurette and Gregoriev, 2005). Thus we may consider feature B in the WV image shown in Fig. 5a to be an indication of upper level moisture and clouds. Hence there may be errors in the NWP moisture fields in the cloud head region, justifying a reduction of PV at upper levels, e.g. at 400 hPa, in region B.

At A in Fig. 5a PV contours are adjusted to form a more pronounced cyclonic pattern over the darkest region at pressure levels 300, 400 and 500 hPa. At C low level PV is enhanced at levels 800 and 900 hPa, by  $\sim 1\text{--}1.5$  PVU. This is justified by the well developed cloud head which indicates ascent of the warm and moist air and consequently a stronger low level PV anomaly at the cyclone centre and associated front than the  $\sim 1$  PVU originally present. The SV signal is very strong and spatially confined at these levels (Figs. 4c and f), also supporting PV modification there. Figure 5b shows the WV image with the 400 hPa (bold contours) and 800 hPa (dashed contours) modified PV field superimposed.

(ii) The modified PV field is now inverted, providing fields of geopotential heights and winds, which together with RH fields (the same as in the CONTROL analysis) yield the new numerical analysis. If necessary, the PV magnitudes are modified further and PV inversion carried out until the height field is as consistent as possible with the observations. The surface pressure fields for the modified (solid contours) and the control (dashed contours) analyses are shown in Fig. 6b. Though there is not a perfect agreement with the observations, there is some improvement over CONTROL in the vicinity of the developing cyclone. The difference between the two analyses is smaller in the regions farther north and east.

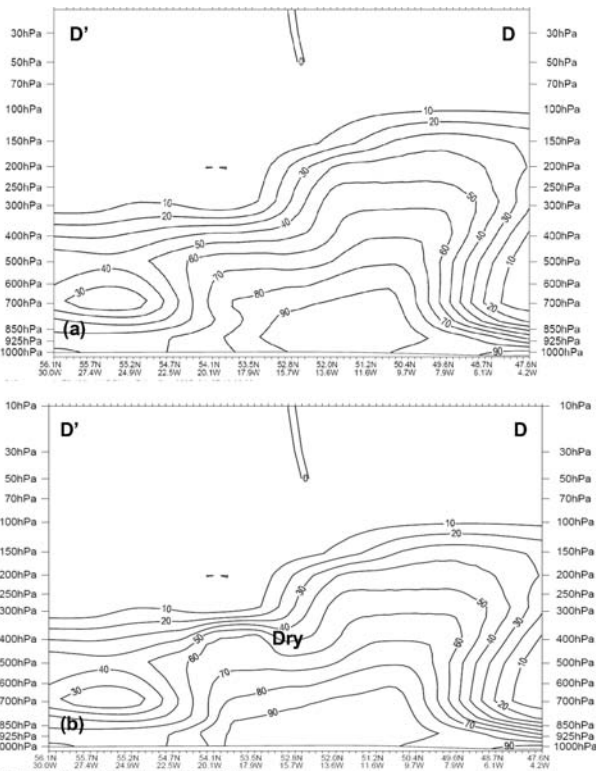


Fig. 7. (a) Control analysis of relative humidity along the cross-section DD', at 18 UTC on 7 January 2005. Location shown in Fig. 5a. (b) As for (a), but modified relative humidity fields. The region of relatively dry air is indicated.

(iii) A rerun, referred to as EXP1, based on the new analysis, is now carried out. Figure 6c shows the modified (EXP1) 18 h forecast at 12 UTC on 8 January. The central pressure is now only slightly higher than observed (~2 hPa), cf. Fig. 2c. Also noteworthy are the simulated strong winds in the North Sea, and weaker winds close to the cyclone centre at the west coast of Norway, in Fig. 6c. This wind pattern is in agreement with the observed, as shown in Fig. 2c.

**7. Sensitivity tests**

In the previous section upper level PV was modified according to WV signals while SV information was used as support in determining the three-dimensional structure of the modification. Low level PV was enhanced in regions covered by the polar front cloud band, a very bright feature in the WV image (Fig. 5). Since the structure and location of low level PV anomalies are difficult to assess based on the WV image alone, we have adopted the following procedure in modification of low level PV anomalies:

(i) A tentative identification of such anomalies can be made by referring to experience and general knowledge of atmospheric dynamics visualized by conceptual models, applied to the actual NWP analysis fields.

(ii) A further tool is provided by the SVs which in this case strongly indicated the same region as sensitive as inferred in (i).

The PV modifications performed in EXP1 were partly based on SV information. We consider the sensitive regions described in EXP1 as the most important ones for the following reasons:

(1) Inspection of traditional observations west and southwest of Ireland, such as synops, indicates incipient cyclogenesis.

(2) The signal seen in the WV image clearly points to this region as dynamically active, that is, a darkening of the dark feature in the WV image, indicating descent of PV-rich stratospheric air and at the same time a brightening of the bright feature showing the cloud head, an indication of ascent of moist air.

(3) As mentioned in Section 5, the low level SV signal is rather focused at the low level baroclinic zone and the upper level SV signal is strong upshear of the low level SV signal and baroclinic zone, indicating the baroclinic structure of the flow in this region. The upper level SV signal also coincides well with the location of the developing WV feature.

As the SV signal at upper levels is spread out over a large regions, local modification of PV distant from the dynamically active region may also have an impact on the cyclone development.

In order to test the relevance of the SVs as an additional tool in PV modification and the impacts on numerical simulations from modifying the RH fields, we now give a description of some additional test runs.

The various simulations performed in this study are presented briefly in Table 1.

(1) In EXP2 we test the impact of the low level PV located in the strongly sensitive and dynamically active region at Ireland

Table 1. Simulations of the 7–8 January 2005 winter storm

OPHIR	Operational HiRLAM run at 12 UTC on 07.01.2005.
REHIR	HiRLAM simulation at 18 UTC on 07.01.2005, using ECMWF boundary fields.
CONTROL	Simulation at 18 UTC on 07.01.2005, based on inversion of original initial PV fields.
EXP1	Simulation at 18 UTC on 07.01.2005, based on inversion of modified initial PV fields in dry intrusion, cloud head and low level frontal PV at the incipient cyclone.
EXP2	As in EXP1, but low level frontal PV associated with the incipient cyclone is left unchanged.
EXP3	As in EXP1, but PV in the sensitive region at E, location shown in, for example, Figs. 4b and 8c is modified.
EXP4	As in EXP1, but RH fields modified to be consistent with PV modifications.
EXP5	As in EXP1, but RH fields reduced to 0.5 percent or less in the whole integration region 2 shown in Fig. 1.

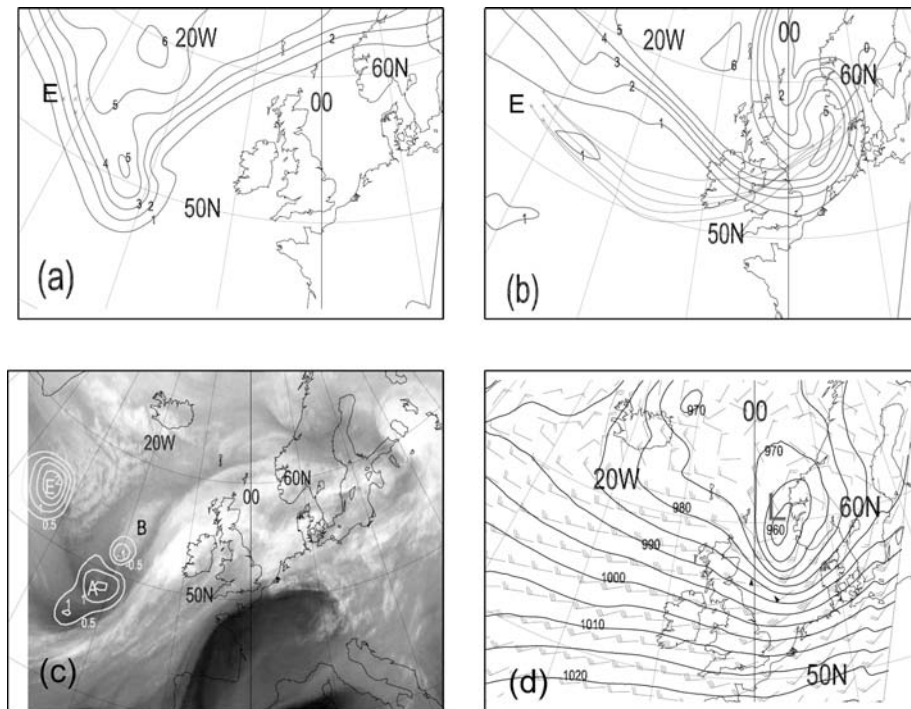


Fig. 8. (a) The EXP3 analysis of PV on the 305 K isentropic surface, contour interval 1.0 PVU, at 18 UTC on 7 January. The initial positions for trajectory calculations, radius 100 km, are shown at E. (b) The EXP3 18 h forecast of PV and trajectories on the 305 K surface at 12 UTC on 8 January. (c) Difference between modified (EXP3) and original (CONTROL) PV field on the 400 hPa surface, superimposed on the METEOSAT7 WV image. Contour interval 0.5 PVU. (d) 18 h EXP3 forecast of surface pressure and 10 m winds.

(Figs. 4c and f). This is done by leaving low level PV at 800 and 900 hPa unchanged, while PV modification at upper levels is as in the modified run, EXP1, described in Section 6.2. Figure 6d shows the EXP2 +18 h simulation of the cyclone. Central surface pressure in this case is slightly higher than in the EXP1 simulation. The storm is lagging behind and is located south of its position shown in EXP1 (Fig. 6c) and in the synoptic analysis (Fig. 2c).

(2) In EXP3, upper level PV at 300–500 hPa is enhanced in the region of the mid - North Atlantic, bounded by 30–40°W, 51–57°N. This change of the PV field is performed in a region where the leading SVs show maximum upper level signal. The region is indicated by the letter 'E' in Figs. 4b, e and 8a–c. Elsewhere PV is modified as in EXP1.

The WV signal in this region is less distinct than in the baroclinic zone west of Ireland. There are upper level clouds and moisture within the deep cold air in this region, all contributing to a rather weak contrast between PV-rich stratospheric air and the surrounding tropospheric air mass. We also observe that the region at E is not dynamically active at the time of modification.

In order to demonstrate why this winter storm is highly sensitive to changes of the mid- and upper-level flow in region E, we now study trajectories starting in this region. Figure 8a shows the EXP3 analysis of the PV field on the 305 K isentropic surface, at 18 UTC on 7 January, while initial positions of se-

lected air parcels on the 305 K surface at this time are indicated (by crosses) at E. The radius of the circle encompassing the positions is 100 km and the selected air parcels are located at 340–370 hPa levels. Figure 8b shows the EXP3 18 h simulation of the PV field and trajectories on the 305 K surface, valid at 12 UTC on 8 January. The trajectories all end within the pronounced upper level PV anomaly associated with the cyclone, over the eastern part of the North Sea. The selected air parcels are at this time located at levels 375–480 hPa.

Hence PV rich air from upper levels at E descends nearly adiabatically in the westerly flow and contributes to the strength of the PV anomaly 18 h later.

Figure 8c shows the difference between the modified and original PV field at the 400 hPa surface, superimposed on the WV image. Figure 8d shows the result from the EXP3 18 h simulation of the storm. The position is quite well forecast, but the cyclone is stronger than observed with central surface pressure at ~958 hPa and generally lower surface pressure than observed within a large region west of Norway and over the North Sea.

(3) A fourth experiment, EXP4, was carried out with the same PV modifications as described in the case of EXP1 in Section 6.2, but with relative humidity (RH) fields adjusted initially, according to the WV image and consistent with the corrected upper level PV fields. Such a distribution of PV and RH is ascribed to ascent of moist air as described in Section 6.2. The

ascent of moist air, creating the cloud head, takes place along the sloping frontal surface and is due to moist symmetric instability, also referred to as slantwise convection (e.g. Shutts, 1990).

The RH field is now enhanced to more than 60% at 400–500 hPa in the cloud head region, the location of which is observed in the satellite image. Furthermore the RH field was enhanced by ~10–15% at 700–1000 hPa levels below the cloud head. The modified RH distribution is indicated by the sloping structure towards the cold air with enhanced RH at 400–500 hPa and below 700 hPa levels presented in Fig. 7b. We believe that this moisture distribution is closer to the initial distribution in cloud head regions observed in successful NWP simulations of strong cyclogenesis (e.g. Santurette and Georgiev, 2005). We also observe that the cloud head is separated from the polar front cloud band, reaching 200–250 hPa levels, by a slot of relatively drier air, indicated in Fig. 7b at 16°W. These features are observed in the satellite image along the line DD' in Fig. 5a, showing a feature of darker grey shades associated with the dry intrusion, between the very bright polar front cloud band (C) and the cloudhead (B).

There were essentially no effects from the modified RH field on this model rerun compared to the rerun described in EXP1 (not shown). This result is in agreement with previous experiments where the effects from initial RH modifications were negligible (Røsting and Kristjánsson, 2006). On the other hand, abundant moisture content is of course vital for strong cyclogenesis.

(4) In EXP5 the initial RH field was reduced to 0.5% or less at all levels within the integration region (region 2 shown in Fig. 1), while PV modifications were as in EXP1. The simulated cyclone development was in this case much weaker, with central surface pressure at +18 to +30 h reaching ~970 hPa, i.e. ~10 hPa higher than in the EXP1 run (not shown). Hence, at least ~30% of the deepening could be attributed to release of latent heat in this case.<sup>3</sup>

## 8. DISCUSSION

Modification of the PV fields in the numerical analysis seems to be a promising method for improving short range simulations in cases with large analysis errors. This is probably the only method which can be adopted manually to produce a consistent new analysis designed for an immediate resimulation. However, the selection of regions subject to modification is uncertain when based on the PV-WV relationship only. Though the satellite imagery may clearly indicate the required geographical area subject to PV modification, the vertical structure of a PV anomaly modification may be ambiguous and uncertain as different vertical

structures of a PV anomaly may, by PV inversion, yield essentially the same analysis in terms of, for example, surface pressure. However, when manually introducing changes in the numerical analysis one wants to include levels which are sensitive to new data. By using an objective method, such as SV analysis, as support for PV modification, the problem of determining the structure of a PV modification is alleviated substantially. On the other hand, as mentioned above in Section 2.2, SVs are not a perfect tool in all cases. In the present study the leading SVs appear to highlight properly the real sensitive regions, i.e. regions where small changes in the PV field have a significant impact on the model reruns. However, there are other cases, involving serious forecast failures, where the SVs were calculated based on poor analyses. In such cases the leading SVs may fail to highlight the true sensitive regions (e.g. Buizza and Montani, 1999; Montani et al., 1999).

### 8.1. PV modifications in sensitive regions

In the case of the winter storm discussed in this paper, one would in an operational environment focus on the sensitive region southwest of Ireland, as this region is dynamically active. Enhancing PV in area E, which is highlighted as strongly sensitive, has a notable effect on the numerical simulation of the cyclone, though the effect turned out to be detrimental to the forecast, by deepening the cyclone too much. However, this experiment was designed to test the sensitivity of the cyclone development to PV changes at upper levels at E, not necessarily to improve the simulation. The effects on the cyclone from the PV anomaly in region E illustrates the complex pattern of events contributing to cyclogenesis. Occasionally the train of events creating strong cyclogenesis also includes the effects from downstream developments, as discussed below.

### 8.2. The role of the initial moisture field

As mentioned in Section 2.4, the SV calculations in this study have been performed by the T42L31 spectral model, that is, spectral truncation at wavenumber 42 and performed with simplified physics, i.e. retaining vertical diffusion and surface drag only. Hence moist processes are not included in these SV calculations, and this may also contribute to inaccurate targeting.

Coutinho et al. (2003) have calculated SVs by a T63L31 model with full physics, based on the total energy norm. The results from their experiments revealed a strong impact from the moist processes (release of latent heat) on the structure and growth of the SVs.

Investigations by Coutinho and Hoskins (Special Project SPGBDSV, 2003, available on the web) have calculated SVs by the T63L31 model with full physics, with a norm that allows initial perturbations in the moisture field. Though the SV-amplification was larger than for the calculations mentioned above, the structure of the SVs were not much different.

<sup>3</sup>The diabatic effects were not 'turned off' in this simulation, hence the RH fields were partly restored at low levels during the simulation out to 24–30 h. Moisture was advected across upstream integration boundaries at all levels.

These results are partly in agreement with those from EXP4 and EXP5 in Section 7, that abundant moisture is crucial for rapid cyclogenesis, though local errors in the moisture field in a NWP analysis seem to be less important. The reason is that the moisture field is modulated by the dynamical processes. Though there may be initial inconsistencies in the moisture field in the NWP analysis, these will rapidly be adjusted to become consistent with the flow structures. After onset of cyclogenesis however, the moisture distribution will affect the dynamical processes as a positive feed back mechanism. An illustration of such an impact from the local humidity-distribution on strong cyclogenesis is the redistribution of PV due to release of latent heat, a processes described by eq. (2) and the related discussion in Section 2.1 and EXP4 in Section 7.

One may speculate if initial modification of the moisture field would have an effect on the simulation if it was introduced after the onset of strong cyclogenesis.

### 8.3. PV modification and ensemble forecasting

The experiments based on PV modifications described in Sections 6 and 7 may suggest the possibility of adopting this technique in preparing ensemble forecasts in the short range.

When SVs are applied to atmospheric dynamics we have assumed that their structure and development can be described by PV anomalies, as indicated by relation (3). Traditionally SV and PV dynamics have been regarded as highly different and partly conflicting approaches to atmospheric sensitivity studies. SVs seem to focus on sensitive regions in the lower troposphere, while PV-thinking focuses on upper tropospheric levels and levels close to the surface.

In order to try to close the apparent gap between SV and PV thinking we may observe the following items:

(1) Relation (3), when combined with the thermodynamic energy equation and geostrophic balance, is the basis for the Eady model which provides a classical description of baroclinic instability.

(2) The local change of the zonal average of the perturbation PV,  $\partial \bar{q}' / \partial t$ , where  $\partial q' / \partial t$  is described by relation (3), is related to the divergence of the Eliassen–Palm flux, which essentially describes the effects from energy propagation from low level perturbations of the flow to the tropopause.

(3) The local change of ‘wave activity density’ describes how  $\bar{q}'$  is propagated by the group velocity.

Cfr. also Morgan (2000) for an extensive treatment of the relation between SV and PV dynamics.

Hence relation (3), describing the change of a PV perturbation, is consistent with the requirements of SV dynamics. There are theoretical justifications for describing SVs by relation (3) and introducing perturbations in the PV field in sensitive regions, by which perturbed analyses for ensemble forecasts can be prepared.

By the method presented in this research analyses for short range ensemble forecasts could be done as follows:

(i) By interactive methods in real time, PV modifications can be performed in sensitive regions, indicated by the fastest growing SVs. Contrary to perturbations introduced for operational ensemble forecasting, the PV modifications have to be fairly large in order to have a notable effect on the short range simulation.

(ii) PV inversion then produces a perturbed analysis.

(iii) Model simulations based on the perturbed analyses are carried out to produce the ensemble members.

In order to produce ensemble members it may be necessary to run the simulations for a much larger integration region than the one used in the present experiments (Fig. 1) in order to suppress the impacts from the boundary fields. However, even in the case described in this study, there were distinct differences in the experimental forecasts, depending on the initial PV modifications, out to 36 h.

### 8.4. Further limitations of the PV modifications in improving the numerical reruns

There are some general limitations of the PV inversion method, beside the technical difficulties of negative PV and lack of divergent winds in inverted fields mentioned in Section 2.4. These limitations are related to mesoscale flow on the one hand and the flow on the synoptic scales on the other.

(1) On the mesoscale the leading edge of the dry intrusion, with its associated stratospheric PV, generally undercuts the frontal cloud band (Browning, 1997, 2005). This part of the PV field is not modified in our experiments, since its structure is difficult to infer from the satellite imagery. However, modification in such regions may be supported if they are sensitive to modifications, i.e. sensitive according to the leading SVs. PV in such a low level part of a dry intrusion is, according to several case studies, probably reduced to far below 2 PVU (e.g. Figs. 6 and 9 in Browning, 1997) by turbulent mixing.

(2) For the synoptic scales the amplitudes of the upper level PV anomalies are often a consequence of a downstream development, and the beneficial effects from PV modification seem to be smaller than otherwise, cf. for example, Persson (2002) for a thorough discussion on downstream developments.

In order to explain the possible limitations of the benefit from PV modifications in cases of downstream cyclogenesis, we now describe the PV perspective of such developments.

Figure 9 shows schematically horizontal charts with 300 hPa geopotential heights in light contours while selected PV iso-lines are shown by thick contours. The development of the flow described below is visualized to take place relative to the cyclone at A. West and east are indicated by letters W and E, respectively. As only one pressure level is presented in Fig. 9, we assume that conditions are baroclinic with vertical wind shear. Hence in

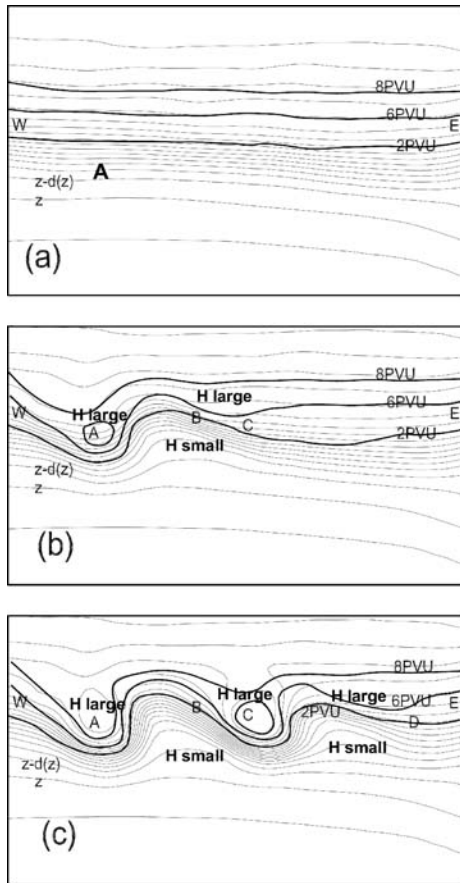


Fig. 9. Schematic presentation of upper level (300 hPa) geopotential heights (light contours) and PV field indicated by selected contours in bold isolines. The fields are shown during cyclogenesis and also show downshear impacts. West and east are indicated by W and E, respectively. Regions with high and low values of the Rossby penetration height ( $H$ ) are indicated. (a) Initial zonal flow pattern at time  $t_0$ . (b) Developing upper level wave at time  $t_1$  due to cyclogenesis at A and the formation of an upper level jet at B, with left-hand jet exit at C. (c) Amplification of the upper level wave at time  $t_2$  associated with downshear cyclogenesis at C and the formation of an upper level jet west of D with left-hand jet exit at D.

the following discussion we use the expressions downshear (up-shear) rather than downstream (upstream). Typical regions with high and low values of the Rossby penetration height ( $H$ ) are indicated in the figure. This height is given (in quasi-geostrophic sense) by  $H = fL/N$ ,  $f$  being the Coriolis parameter,  $L$  the characteristic horizontal dimension of the perturbation and  $N^2$  the Brunt-Vaisala frequency, expressing static stability.

Figure 9a shows a zonal flow at an initial time  $t_0$ . We now assume that cyclogenesis takes place in the western section of the flow, at location A, starting with a low level wave (created by e.g. differential diabatic heating due to sea-land contrasts). The thermal circulation associated with the low level wave creates an upper level wave, provided that  $H$  is large enough (e.g. Hoskins

et al., 1985). Such an upper level wave is in a favourable position upshear of the low level cyclone centre for further mutual intensification of the upper and lower level waves, a process referred to as ‘self development’.

Results from this kind of process is indicated in Fig. 9b showing the developing upper level wave in the region A–B at a later time  $t_1$ . The warm advection associated with the cyclogenesis will enhance the upper level jet at B, by which a left-hand exit region of this jet appears at C. In the presence of a low level baroclinic zone, cyclogenesis takes place at C (this time initiated at upper levels). Cyclogenesis in the left exit region of an upper level jet is rapid due to large  $H$ .

Figure 9c shows the strong upper level PV anomaly at C due to this left-hand exit development at the later time  $t_2$ . A new sharpening of the jet takes place east of the new ridge, possibly spawning a new downshear development in the new left-hand exit at D.

Slightly north of region B in Fig. 9b, in the left-hand inflow of the jet, descent of dry high-PV stratospheric air takes place. This air flows into region C, forming a positive PV anomaly interacting with the low level baroclinic zone. Such a process can clearly be inferred from features in the WV image as discussed in Section 6.

We now assume that Fig. 9 represents NWP analyses at times  $t_0$ – $t_2$ . A correction of an observed mismatch between the PV fields and features in the WV image in region C at time  $t_1$  may in this case have a limited beneficial effect on a numerical rerun. This is because the analysis error at C at  $t_1$  (and hence wrong location of the PV field at C) is strongly influenced by errors in the NWP analysis at A at times  $t_0$  and  $t_1$ . If the NWP model fails to simulate the development at A, it will fail to predict properly the development at C. Hence the background field adopted for the NWP analysis at  $t_1$  would contain errors in regions A and C.

In this case lower levels at A could be an important sensitive region, highlighted by the fastest growing targeted SVs, with C as verification area. Correction of the PV field in the lower troposphere at A (target region) could improve the forecast of the downshear development at C.

To what extent PV modifications in cases of downshear developments are less successful than otherwise remains, however, uncertain and may be subject to further investigations.

## 9. Conclusion

In this study we have investigated the winter storm of 7–8 January 2005. This storm affected large parts of northern Europe, and even though it was rather well forecast by operational NWP models, there was some uncertainty about the cyclone track, even in the short range forecasts. A possible error in the upper level PV field, as compared to the features in the WV satellite image, motivated modifications of the PV fields in the NWP analysis. SV analysis was invoked in the process, by adjusting the PV fields at sensitive levels where new information is expected

to have a large impact on the numerical simulation. Hence the three dimensional structure of the modification was determined by less ambiguity than with a pure trial and error method which otherwise would have to be adopted. Inversion of the modified PV field, followed by a rerun based on the resulting modified initial state produced a substantially improved simulation of the 7–8 January storm. Even the mesoscale structure of the central part of the cyclone (seen by comparison of Figs. 2c and 6c) was successfully simulated.

The strength of the method of manually correcting the PV fields, as described in this and several other studies, can partly be ascribed to the nearly one to one correspondence between features in WV images and in upper level PV fields in the baroclinic zones. Hence errors are easily detected qualitatively by a mere superposition of the PV fields in the numerical analysis on the imagery, a procedure easily performed on a workstation (such as used in the DIANA system). The information derived from the WV images is, by correction and inversion of PV fields, translated directly into dynamically consistent fields, readily available in a numerical rerun without invoking data assimilation. The method also allows large modifications of the flow. Such modifications might be rejected by the data assimilation routines if they deviate too much from the error statistics contained in the analysis error covariance matrix.

Correction of RH fields appears to have a negligible effect on the simulation. The initial lack of consistency between modified PV and original RH fields rapidly disappears, after 3–6 h of simulation time.

There are still comparatively few cases serving as documentation of the true benefits of manual intervention in numerical analyses, such as described in this research. The improved resimulation of the 7–8 January storm was carried out with the benefit of hindsight. However, there has been a fairly large number of investigations adopting initial PV modification, and they have all yielded promising results (Demirtas and Thorpe, 1999; Røsting et al., 2003; Hello and Arbogast, 2004; Verkley et al., 2005; Røsting and Kristjánsson, 2006). At MI the new digital analysis system (DIANA) has been modified to allow modification of PV and RH fields interactively. Thus the time needed to perform PV modifications and model reruns is now short enough for implementation in an operational environment. Future research in this field will involve real time experiments. A version of the HiRLAM similar to the operational model will be used for this purpose during a test period. A semi-operational routine at MI for such real time experiments for the autumn and winter seasons 2008–2009 is currently taking place.

## 10. Acknowledgements

The basic inversion routine used in our research was originally supplied by Christopher A. Davis, and the PV inversion package was supplied by Sigurdur Thorsteinsson and co-workers at the Icelandic Meteorological Office. The software for calculating the

PV structure of singular vectors was provided by Andrea Montani. The late Anstein Foss modified the necessary software for doing PV inversions at the Norwegian Meteorological Institute (MI). Members of the division for research and development at MI developed the DIANA system, which for the purpose of this study has been modified to include editing of PV and RH fields interactively.

## References

- Appenzeller, C. and Davies, H. C. 1992. Structure of stratospheric intrusions into the troposphere. *Nature* **358**, 570–572.
- Bishop, C. H., Etherton, B. J. and Majumdar, S. J. 2001. Adaptive sampling with the ensemble transform Kalman filter. Part 1: theoretical aspects. *Mon. Wea. Rev.* **129**, 420–436.
- Bouttier, F. and Kelly, G. 2001. Observing-system experiments in the ECMWF 4D-Var data assimilation system. *Q. J. R. Meteorol. Soc.* **127**, 1469–1488.
- Browning, K. A. 1997. The dry intrusion perspective of extra-tropical cyclone development. *Meteorol. Appl.* **4**, 317–324.
- Browning, K. A., 2005. Observational synthesis of mesoscale structures within an explosively developing cyclone. *Q. J. R. Meteorol. Soc.* **131**, 603–623.
- Browning, K. A., Thorpe, A. J., Montani, A., Parsons, D., Griffiths, M. and co-authors. 2000. Interactions of tropopause depressions with an ex-tropical cyclone and sensitivity of forecasts to analysis errors. *Mon. Wea. Rev.* **128**, 1734–1755.
- Buizza, R. and Palmer, T. N. 1995. The singular vector structure of the atmospheric global circulation. *J. Atmos. Sci.* **52**, 1434–1456.
- Buizza, R. and Montani, A. 1999. Targeting observations using singular vectors. *J. Atmos. Sci.* **56**, 2965–2985.
- Charney, J. G. 1955. The use of the primitive equations of motions in numerical prediction. *Tellus* **7**, 22–26.
- Coutinho, M. and Hoskins, B. 2003. Moist Singular Vectors, Third Report, Special Project SPGBDSV, available on the web.
- Coutinho, M. M., Hoskins, B. J. and Buizza, R. 2003. The influence of physical processes on extratropical singular vectors. *J. Atmos. Sci.* **61**, 195–209.
- Davis, C. A. 1992. Piecewise potential vorticity inversion. *J. Atmos. Sci.* **49**, 1397–1411.
- Davis, C. A. and Emanuel, K. A. 1991. Potential vorticity diagnostics of cyclogenesis. *Mon. Wea. Rev.* **119**, 1929–1953.
- Demirtas, M. and Thorpe, A. J. 1999. Sensitivity of short range weather forecasts to local potential vorticity modifications. *Mon. Wea. Rev.* **127**, 922–939.
- ECMWF Newsletter No 83-1999. PrepIFS-Global modelling via the Internet.
- Hello, G. and Arbogast, P. 2004. Two different methods to correct the initial conditions applied to the storm of 27 December 1999 over southern France. *Meteorol. Appl.* **11**, 41–57.
- Hoskins, B. J., McIntyre, M. E. and Robertson, A. W. 1985. On the use and significance of isentropic potential vorticity maps. *Q. J. R. Meteorol. Soc.* **111**, 877–946.
- Jung, T., Klinker, E. and Uppala, S. 2005. Reanalysis and reforecast of three major European storms of the twentieth century using the ECMWF forecasting system. Part 2. Ensemble forecasts. *Meteorol. Appl.* **12**, 111–122.

- Kalnay, E. 2003. *Atmospheric Modeling, Data Assimilation and Predictability*. Cambridge University Press, Cambridge, ISBN 0521 79629 6, pp. 205,253.
- Kristjánsson, J. E., Thorsteinsson, S. and Ulfarsson, G. F. 1999. Potential vorticity based interpretation of the 'Greenhouse Low', 2–3 February 1991. *Tellus* **51A**, 233–248.
- Majumdar, S. J., Bishop, C. H., Buizza, R. and Gelaro, R. 2002. A Comparison of ensemble-transform Kalman-filter targeting guidance with ECMWF and NRL total-energy singular-vector guidance. *Q. J. R. Meteorol. Soc.* **128**, 2527–2549.
- Mansfield, D. 1996. The use of potential vorticity as an operational forecasting tool. *Meteorol. Appl.* **3**, 195–210.
- Montani, A. 1998. *Targeting of Observations to Improve Forecasts of Cyclogenesis*. PhD Thesis. University of Reading.
- Montani, A., Thorpe, A. J., Buizza, R. and Uden, P. 1999. Forecast skill of the ECMWF model using targeted observations during FASTEX. *Q. J. R. Meteorol. Soc.* **125**, 3219–3240.
- Morgan, C. M. 2000. A Potential Vorticity and Wave Activity Diagnosis of Optimal Perturbation Evolution. *J. Atmos. Sci.* **58**, 2518–2544.
- Persson, A. 2002. *Atmospheric Motions*. Volume 1: The Earth System: Physical and Chemical Dimensions of Global Environmental Change. Encyclopedia of Global Environmental Change, John Wiley and Sons, Chichester, ISBN 0471-97796-9, 221–242.
- Petersen, G. N., Majumdar, S. J. and Thorpe, A. J. 2007. The properties of sensitive area predictions based on the ensemble transform Kalman filter (ETKF). *Q. J. R. Meteorol. Soc.* **133**, 697–710.
- Rabier, F., Jarvinen, E., Klinker, E., Mahfouf, J. F. and Simmons, A. 2000. The ECMWF operational implementation of four-dimensional variational assimilation. I: Experimental results with simplified physics. *Q. J. R. Meteorol. Soc.* **126**, 1143–1170.
- Røsting, B. and Kristjánsson, J. E. 2006. Improving simulations of severe winter storms by initial modification of potential vorticity in sensitive regions. *Q. J. R. Meteorol. Soc.* **132**, 2625–2652.
- Røsting, B., Kristjánsson, J. E. and Sunde, J. 2003. The sensitivity of numerical simulations to initial modifications of potential vorticity – a case-study. *Q. J. R. Meteorol. Soc.* **129**, 2697–2718.
- Santurette, P. and Georgiev, C. G. 2005. *Weather Analysis and Forecasting, Applying Satellite Water Vapor Imagery and Potential Vorticity Analysis*. Elsevier Academic Press, London, ISBN: 0-12-619262-6.
- Shapiro, M., Wernli, H., Bao, J. W., Methven, J., Zou, X. and co-authors. 1999. A planetary-scale to mesoscale perspective of the life cycles of extratropical cyclones: the bridge between theory and observations. In: *The Life Cycles of Extratropical Cyclones*. American Meteorological Society, Boston, ISBN 1-878220-35-7, 139–185.
- Shutts, G. J. 1990. Dynamical aspects of the October storm, 1987: A study of a successful fine-mesh simulation. *Q. J. R. Meteorol. Soc.* **116**, 1315–1347.
- Verkley, W. T. M., Vosbeek, P. W. C. and Moene, A. R. 2005. Manually adjusting a numerical weather analysis in terms of potential vorticity using three dimensional variational data assimilation. *Q. J. R. Meteorol. Soc.* **131**, 1713–1736.
- Weldon, R. B. and Holmes, S. J. 1991. Water vapor imagery: interpretation and applications to weather analysis and forecasting, NOAA Technical Report, NESDIS 57, NOAA, US Department of Commerce, Washington D. C., 213 pp.
- Young, M. V., Monk, G. A. and Browning, K. A. 1987. Interpretation of a rapidly deepening cyclone. *Q. J. R. Meteorol. Soc.* **113**, 1089–1100.